ACS APPLIED MATERIALS & INTERFACES

Research Article

Cite This: ACS Appl. Mater. Interfaces XXXX, XXX, XXX−XXX

www.acsami.org

Effect of Metal Electrodes on Aging-Induced Performance Recovery in Perovskite Solar Cells

Dong Geon Lee,[†,⊥] Min-cheol Kim,[‡,⊥] Shen Wang,[‡] Byeong Jo Kim,[†,§] Ying Shirley Meng,[*,‡,∥] and Hyun Suk Jung[*,†]

[†]School of Advanced Materials Science & Engineering, Sungkyunkwan University, Suwon 16419, Republic of Korea

[‡]Department of NanoEngineering and [∥]Materials Science and Engineering Program, University of California, San Diego, 9500 Gilman Drive, La Jolla, California 92093, United States

[§]Department of Chemistry, Ångström Laboratory, Uppsala University, Box 523, SE 75120 Uppsala, Sweden

Supporting Information

ABSTRACT: For commercialization of perovskite solar cells (PSCs), it is important to substitute the alternative electrode for Au to decrease the unit cost. From the early stage, Ag exhibits a potential to be a good counter electrode in PSCs; however, there is an abnormal s-shaped $J-V$ curve with the Ag electrode, and it is recovered as time passes. The perception of the aging-induced recovery process and refutation of the raised stability issues are required for commercial application of Ag electrodes. Herein, we compared the aging effect of PSCs with Ag and Au electrodes and found that only devices with Ag electrodes have a dramatical aging-induced recovery process. We observed the change of photoelectronic properties only in the devices with Ag electrodes as time passes, which mainly contributes to recovery of the s-shaped $J-V$ curve. We verified the work function change of an aged Ag electrode and its mechanism by photoelectron spectroscopy analysis. By comparing the light stability under 1 sun intensity illumination, we can assure the practical stability of Ag electrodes in case of being encapsulated. This work suggests the profound understanding of the aging-induced recovery process of PSCs and the possibility of commercial application of Ag electrodes.

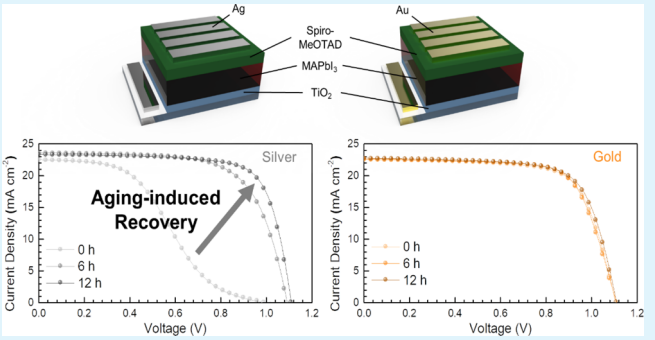

KEYWORDS: *perovskite solar cells, hole injection, work function, interfacial reaction, metal electrodes*

INTRODUCTION

Perovskite solar cells (PSCs) have rapidly improved in terms of their energy-converging performance[1−4] and currently exhibit a power conversion efficiency (PCE) of up to 25.2%.[5] Research on PSCs has been aimed at facilitating commercialization, such as improvements in the long-term stability, scale up of the fabrication process, and improved recycling. Although PSCs have been conceived as economically viable solar cells, efforts should be made to decrease their cost. Compared with polycrystalline silicone solar cells, the price of which is below 0.3 $/Wp, the material and/or fabrication costs of PSCs need to be reduced for commercialization. As one strategy for cost-effectiveness, metal electrode selection is an important consideration. Gold has been reported to be appropriate as a metal electrode for use in PSCs. As a substitute to this expensive metal, various electrodes have been attempted.[6] For example, carbon electrodes have been considered alternative counter electrodes for PSCs; however, they have shown a fairly low efficiency.[7,8] In addition, PSCs with relatively cheap Ag electrodes achieve low PCEs with low open-circuit voltages (V_{OC}) and fill factors (FFs) showing an s-shaped bend in the current-density−voltage ($J-V$) curves for n−i−p PSCs with organic-based hole-transport materials (HTMs). However, with aging, the performance of a PSC recovers to a normal level, and such an abnormal instability can be a significant obstacle for commercial applications of Ag electrodes. $J-V$ curves with s-shaped bends are mainly attributed to an inferior majority charge carrier extraction from the photoabsorbing area to the cathode or anode. However, the underlying reason for these phenomena, particularly for the aging-induced recovery mechanisms in PSCs with Ag electrodes, is yet to be elucidated.

In organic photovoltaics, some studies suggest that the reason for an s-shaped bend in the $J-V$ curve may be attributed to the charge carrier dynamics inside photovoltaic devices.[9,10] Some reports have intrinsically attributed the poor carrier extraction efficiency to a low conductivity, low mobility, or large number of trap states as recombination centers.[11] In contrast, some researchers have blamed the energetic barrier to the charge transport for the low carrier extraction efficiency.[10]

Received: August 15, 2019
Accepted: December 4, 2019
Published: December 4, 2019

DOI: 10.1021/acsami.9b14619
ACS Appl. Mater. Interfaces XXXX, XXX, XXX−XXX

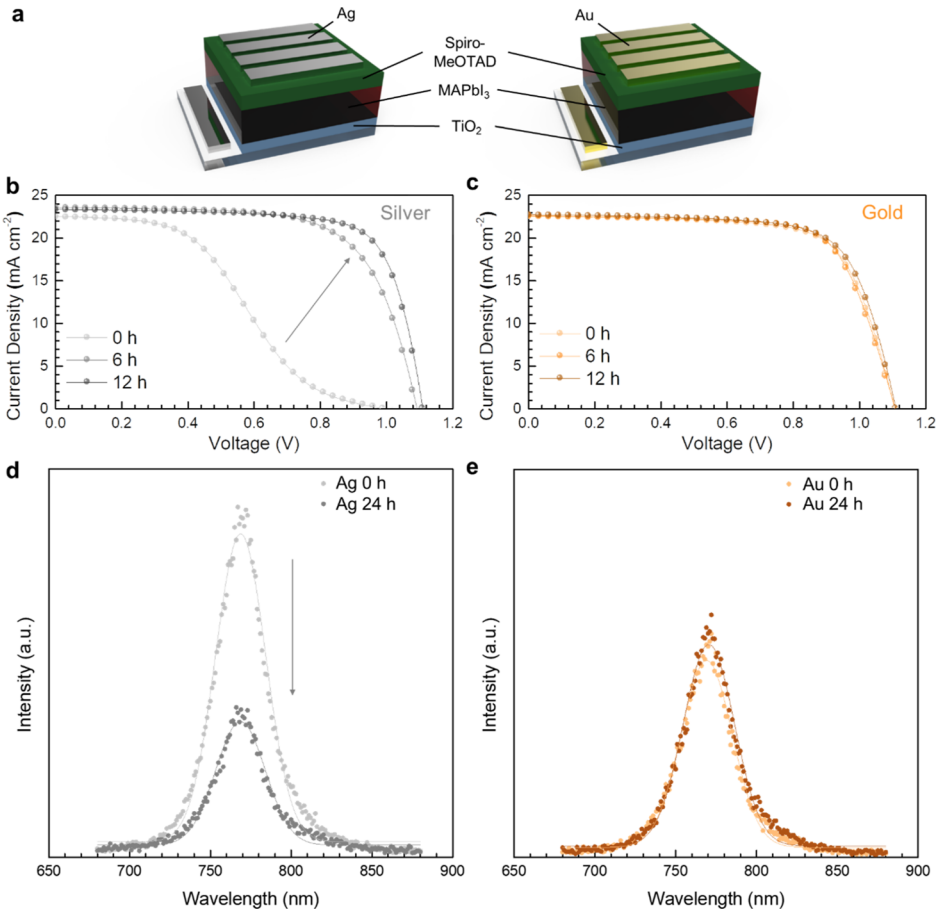

Figure 1. Different aging behaviors of perovskite solar cells depending on the metal counter electrode. (a) PSC device structure (FTO/TiO_2/$MAPbI_3$/spiro-MeOTAD/Ag or Au) and time evolution plot of *J*−*V* curves for PSCs with (b) Ag and (c) Au for their metal counter electrode for different aging times (0, 6, 12 h). PL spectra of fresh (0 h) and aged (24 h) glass/perovskite/spiro-MeOTAD/metal electrode structured device using (d) Ag and (e) Au metal electrodes.

However, in the current use of PSCs, the reason for the recovery of the s-shaped bend with time for the same structure and materials has not been clearly elucidated. It is important to understand the origin of the s-shaped *J*−*V* curves of PSCs with Ag electrodes at an early stage, as well as the aging-induced recovery phenomena through elimination of the s-shaped bends for securing possible use of Ag electrodes in commercialized PSCs.

In the present study, we compare the time-dependent change in the photovoltaic performance of PSCs employing Ag and Au metal electrodes. PSCs with Ag electrodes exhibit a clear s-shaped bend in their *J*−*V* curves during the early stage; however, they recover to their best performance with 12 h of aging. In contrast, PSCs with Au electrodes achieve their best performance from the beginning. To clarify this aging-induced recovery process in PSCs with Ag electrodes, we investigate the alteration of the time-dependent carrier dynamics based on the photoluminescence behaviors as a function of aging. With the aid of photoelectron spectroscopy using X-ray and ultraviolet sources, we first observe that Ag deposited on the spiro-MeOTAD reacted with lithium bis(trifluoromethanesulfonyl)-imide (Li-TFSI) in the spiro-MeOTAD layer and led to work function change of the Ag anode. By analyzing both the measurement and simulation results, we verify that the difference in work function between the Ag and HTMs, spiro-MeOTAD, induces a significant injection barrier for the holes, which clearly causes the formation and alleviation of the s-shaped bend in *J*−*V* curves of PSCs with Ag electrodes. We finally address the potential of Ag electrodes for commercial use by demonstrating highly stable PSCs with Ag electrodes for durations exceeding 350 h under light-illumination, which is close to the results of PSCs with Au electrodes.

MATERIALS AND METHODS

Device Fabrication. The patterned fluorine-doped tin oxide (FTO) substrates (Pilkington TEC15) were cleaned sequentially using acetone, ethanol, and deionized water in an ultrasonic bath for 15 min. A compact TiO_2 (c-TiO_2) layer was spin-coated (3000 rpm, 20 s) on the cleaned FTO substrate using 0.15 M titanium diisopropoxide bis(acetylacetonate) (75 wt % in isopropanol, Sigma-Aldrich) in anhydrous 1-butanol (Sigma-Aldrich). This c-TiO_2 layer was baked at 130 °C for 5 min and then annealed at 500 °C for 30 min. The c-TiO_2/FTO substrate was immersed for 15 min in a 0.04 M $TiCl_4$ solution at 70 °C, rinsed with deionized water, and then annealed at 500 °C for 30 min. The mesoporous TiO_2 (mp-TiO_2) layer was formed by spin-coating (4000 rpm, 30 s) a diluted TiO_2 paste (6:1 ratio, anhydrous 1-butanol/ENB Korea 50 nm TiO_2 paste). The mp-TiO_2-coated substrate was baked at 130 °C for 10 min and then annealed at 500 °C for 60 min.

The perovskite ($CH_3NH_3PbI_3$) layer was coated on the mp-TiO_2 layer by spin-coating (4000 rpm, 20 s) a mixed precursor solution: The solutes (52 wt %) of CH_3NH_3I (Xi'an Polymer Light Technology Co.) and PbI_2 (Alfa Aesar) were at a molar ratio of 1:1.1 in a solvent of dimethylformamide and dimethyl sulfoxide (Sigma-Aldrich) with a volume ratio of 7.33:1. During spin-coating, 0.5 mL of diethyl ether (Sigma-Aldrich) was also dropped onto the precursor film. The spin-

DOI: 10.1021/acsami.9b14619
ACS Appl. Mater. Interfaces XXXX, XXX, XXX−XXX

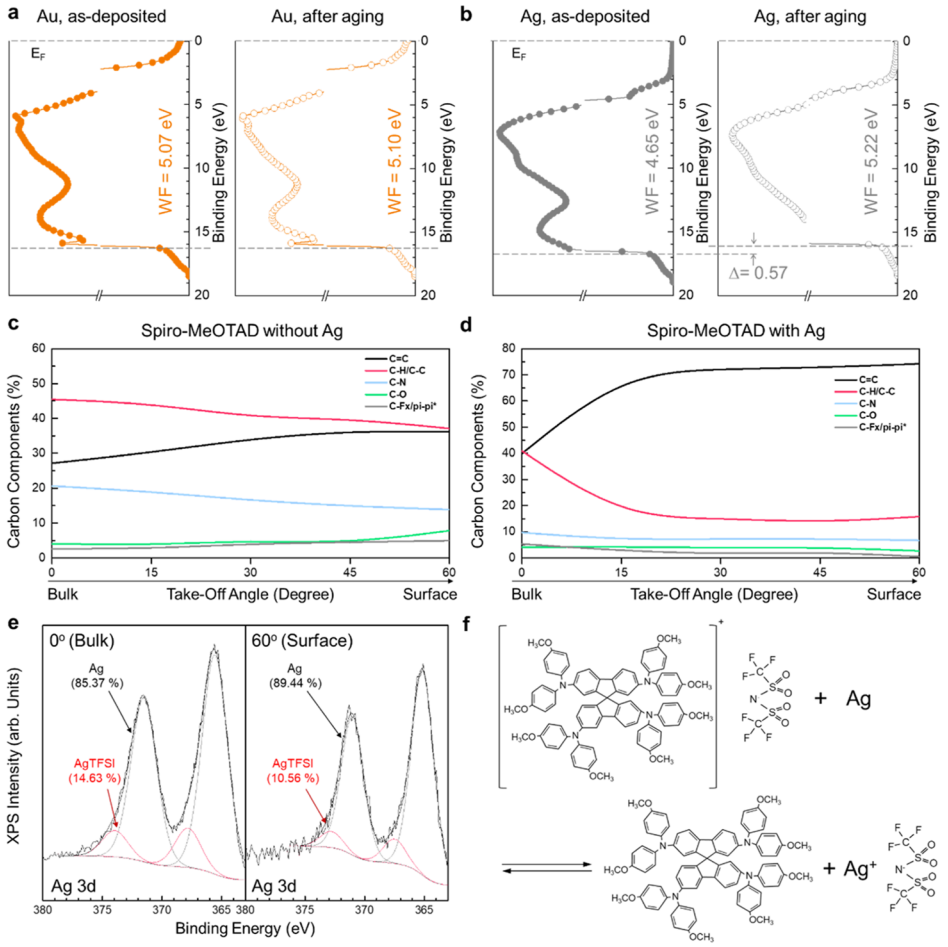

Figure 2. Electrical and chemical changes which lead to the different aging behaviors verified by photoelectron spectroscopy. UPS spectra of (a) Au and (b) Ag on spiro-MeOTAD as-deposited and after aging in the dry air. Carbon components ratio for (c) pristine spiro-MeOTAD and (d) aged Ag-deposited spiro-MeOTAD for 24 h measured from AR-XPS spectra of C 1s. (e) AR-XPS spectra of Ag 3d for Ag-deposited spiro-MeOTAD aged for 24 h. The black line indicates Ag components and the red line indicates Ag^+ components which are from Ag-TFSI. (f) Proposed chemical equation at the interface between Ag and spiro-MeOTAD after Ag deposition.

coated substrate was annealed at 130 °C for 20 min. A hole-transport layer was coated on the perovskite layer by spin-coating as described in a previous report.[12] The Ag and Au electrodes were deposited onto the multilayer substrate using thermal evaporation. The substrate size and active device area were 2 × 2 cm^2 and 0.14 cm^2, respectively.

Aging-Induced Recovery Process. PSCs with an Ag electrode exhibited an abnormal $J-V$ upon the first measurement soon after electrode deposition. The measured PSCs were stored under dark ambient conditions, and an aging-induced recovery process occurred as time passed, resulting in an enhanced performance of the PSCs with an Ag electrode, similar to that using an Au electrode. All experiments including fabrication and aging procedure are conducted inside a dry room with a maintained condition (20 °C, 5% R.H.).

Characterization. The photovoltaic properties were measured using a potentiostat (CHI 600D, CH Instruments) under 1 sun illumination generated by a solar simulator (Newport Oriel Solar 3A Class, 64023A). The light intensity was adjusted using a standard Si solar cell (Oriel, VLSI Standards). The $J-V$ characteristics for all devices were measured at a voltage scan rate of 0.1 V/s. An ultraviolet photoelectron spectroscope equipped with a He I source ($h\nu$ = 21.22 eV) (AXIS Supra, Kratos, UK) was used to measure the energy band of the Ag and Au metal electrodes. Angle-resolved X-ray photoelectron spectroscopy (AR-XPS) was performed using a Kratos AXIS Supra with Al Kα anode source operated at 15 kV and 10^{-8} Torr chamber pressure. Spectra data were calibrated with the hydrocarbon C 1s peak (284.8 eV) and processed by CasaXPS. The steady-state photoluminescence (ss-PL) spectra were measured using a fluorescence spectrophotometer (HITACHI F-7000) equipped with a standard light source (P/N 250-0123) and observed within an entire wavelength range of 680−880 nm. The depth profiles of the PSCs with each metal electrode were analyzed by time-of-flight secondary ion mass spectroscopy (ToF-SIMS-5, ION-TOF).

RESULTS AND DISCUSSION

Mesoscopic PSCs of $MAPbI_3$, which have the same n−i−p structure (FTO/TiO_2/$MAPbI_3$/spiro-MeOTAD/Metal electrode) utilizing different types of metal electrodes (Figure 1a), show different aging trends in the device performance than their metal electrodes, Ag and Au. As can be seen in Figure 1b, PSCs with Ag electrodes exhibit poor performance for the initial measurements soon after device fabrication, with abnormal s-shaped $J-V$ curves. After several hours (6 h), the devices show better performance, but achieve best PCEs after a few more hours (12 h). In contrast, PSCs with Au electrodes exhibit their best performance from the initial measurement and demonstrate a nearly analogous PCE after 6 and 12 h (Figure 1c). Summary of photovoltaic parameters for both PSCs with Ag and Au electrodes is presented in Table S1. These aging-induced recovery phenomena of PSCs with the Ag electrode occur slowly over time when the PSCs are stored in dark and dry conditions (Figure S1).

DOI: 10.1021/acsami.9b14619
ACS Appl. Mater. Interfaces XXXX, XXX, XXX−XXX

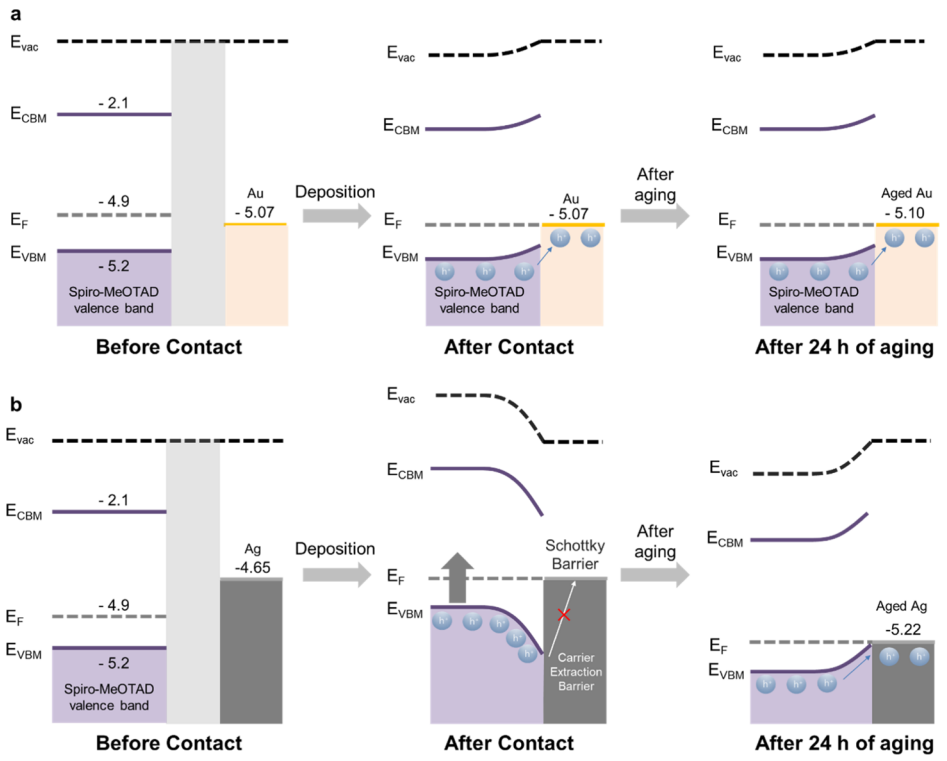

Figure 3. Schematic diagrams for formation of the charge injection barrier mechanism from band bending between spiro-MeOTAD and metal electrodes after aging: (a) Au and (b) Ag.

Regarding this well-known performance instability in organic−inorganic hybrid PSCs, many researchers have stated that material transfer, ion migration, or HTM oxidization could be the origin for such phenomena.[13−16] However, we found that these are minor issues regarding the performance recovery of PSCs with Ag electrodes, as shown in Figures S2 and S3. Figure S2 suggests that a material transfer or ion migration is not the main cause of performance aging when we compare the ion depth profile of PSCs with Ag and Au electrodes using time-of-flight secondary ion mass spectrometry (ToF-SIMS) over time. There are no significant differences between pristine and recovered PSCs for both electrodes, which means there is no significant material transfer or ion migration along each layer. Moreover, we controlled the HTM precursor conditions to verify the oxidization effects, namely, a fresh sample, stored in an ambient and argon atmosphere for 1 day. Similarly, we found that the oxidization of HTMs is also not the main origin of aging because all $J-V$ curves according to the oxidization conditions indicate a similar trend depending on the metal electrodes, and not the oxidization conditions (Figure S3).

The $J-V$ curve of a device with Ag electrodes immediately after fabrication (0 h) implies that the device has a significantly high series resistance. Therefore, we assume that the low V_{OC} and FF during the early stage of a device with Ag electrode can be caused by an inferior charge extraction from perovskite materials to electrodes. To identify more details of the charge extraction in each device, we investigated the photoelectronic properties of devices regarding the metal electrode, using ss-PL measurements. In Figure 1d,e, we can see significant time-dependent changes of the charge transportation in devices with Ag electrodes, whereas devices with Au electrodes show negligible changes over time. For a proper comparison of the electrode effect on the hole transportation, glass/perovskite/spiro-MeOTAD/metal electrode samples were prepared for ss-PL. For a sample with an Ag electrode, the ss-PL spectra show a higher intensity in the as-prepared samples before aging, and after the aging process, the intensity of the ss-PL spectra significantly decreases (Figure 1d). In contrast, a sample with Au electrodes shows identical ss-PL spectra before and after the aging process (Figure 1e). Though ss-PL directly examines the perovskite/HTM interface from the radiative recombination of perovskite layer, the hole accumulation at the HTM/metal electrode interface also influences ss-PL intensity. In that sense, the difference of ss-PL spectra means that the device using an Ag electrode has an inferior hole transport property initially, which is enhanced, reaching a performance analogous with a device using an Au electrode after the aging-induced recovery process.

From the photovoltaic and photoelectronic characteristics of devices with Ag or Au electrodes in Figure 1, we noticed that the charge transport properties to anodes of each device have main differences in the time-evolution depending on metal electrodes. Generally, the carrier injection barrier at a layer interface has been considered to induce the s-shape of a photodiode.[17,18] Consequently, we investigated the electronic structures of PSCs with different metal electrodes under the assumption that there was initially a barrier-interrupting carrier injection owing to energy band bending and that this barrier is relieved over time. To verify the change in electronic structures, we performed ultraviolet photoelectron spectroscopy (UPS) for fresh and aged 3 nm of Au and Ag electrodes deposited on spiro-MeOTAD, which gave us the information about work functions of metal electrodes at the interface as time passed (Figure 2a,b). Identification of each work function was performed using the equation $\Phi = h\nu - E_{cutoff}$, where Φ is the work function, h is the plank constant, ν is the frequency of the radiation, E_{cutoff} is lower kinetic energy (secondary edge).[19,20] As shown in Figure 2a, the Au electrode presents

DOI: 10.1021/acsami.9b14619
ACS Appl. Mater. Interfaces XXXX, XXX, XXX−XXX

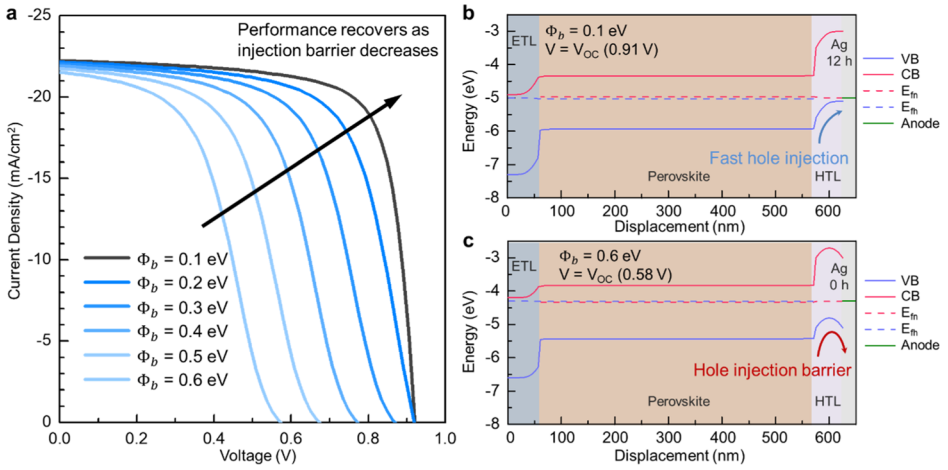

Figure 4. (a) Simulated $J-V$ curves of PSCs depending on various injection barriers (Φ_b = 0.1−0.6 eV), which emulate time-evolutional changes of PSCs with an Ag metal electrode. Simulated energy band diagrams of PSCs including FTO, TiO_2, perovskite, spiro-MeOTAD, and metal electrodes with an injection barrier of Φ_b = (b) 0.1 eV and (c) 0.6 eV at $V = V_{OC}$.

identical photoelectron spectra and work functions (5.07 eV, as-deposited; 5.10 eV, after aging) as-deposited and after the aging process. In contrast, an Ag electrode shows a significant shift in the photoelectron spectra and work function transition of approximately 0.57 eV after aging (4.65 eV, as-deposited; 5.22 eV, after aging). These findings regarding the UPS spectral shift and work function transition of an Ag electrode offer a concrete origin of the inferior performance of as-fabricated PSCs with Ag electrodes and their aging and recovery processes.

To identify such compositional changes which induce the energy level shift, AR-XPS from 0 to 60° for detailed observation on compositional change occurred at the interface between spiro-MeOTAD and ultra-thinly etched (∼1 nm) Ag electrode (Figure S4). For the XPS maximum, acquisition depth is within 10 nm, the coated Ag layer was thinned within 1 nm in order to probe its buried interface. As the coated metal layer still remains on the HTM surface, the potential damage from the Ar^+ plasma to organic HTM was protected by the remaining metal electrode. AR-XPS is a great tool for characterizingthe heterostructure interface,[21,22] because 0° spectra interpret bulk information of materials (∼10 nm of spiro-MeOTAD in this case), and 60° ones interpret interfacial information (∼5 nm interface between spiro-MeOTAD and Ag in this case). The schematics for our detailed AR-XPS measurements according to different take off angles are shown in Figure S5. First, we compared AR-XPS spectra of carbon 1s (C 1s) energies for pristine spiro-MeOTAD and Ag-deposited spiro-MeOTAD after 24 h of aging (Figure 2c,d). The compositional ratio was derived from high-resolution carbon 1s AS-XPS spectra (see Figure S4). Based on these carbon 1s attribution, in spiro-MeOTAD HTM, a clear trend is observed in Figures 2c,d, that the ratio for sp^2 carbon (C═C) composition decrease always associated with the sp^3 carbon (C−C) increase, and vice versa. This is because the HTM oxidation is from the loss of π electrons (sp^2 carbon) on the spiro-MeOTAD's fluorene functional group. The sp^3 carbon signal dominates in oxidized spiro-MeOTAD, and contrary to this, the sp^2 carbon signal dominates in spiro-MeOTAD, which is not oxidized.[23] As can be seen in Figure 2c, spiro-MeOTAD without Ag deposition has more sp^3 carbon, which means more oxidized spiro-MeOTAD was observed on the HTM surface. Ag needs to be diffused through the HTM surface to the bulk, the more oxidized spiro-MeOTAD could be observed near HTM surface. However, in spiro-MeOTAD with Ag deposition (Figure 2d), there is much more sp^2 carbon at the surface near the Ag electrode, which indicates the de-oxidization of spiro-MeOTAD. Previous research shows that Ag-TFSI was applied as the reagent to fully oxidize spiro-MeOTAD, the reaction products being silver and oxidized spiro-MeOTAD (spiro-MeOTAD$^+$TFSI$^-$).[24] Regarding an equilibrium state, the reduction of oxidized spiro-MeOTAD could happen in a silver-rich chemical environment.

AR-XPS spectra of Ag 3d energies for Ag-deposited spiro-MeOTAD present a decisive clue for such de-oxidization of spiro-MeOTAD and work function change of Ag after aging (Figure 2e). Though Ag did not react with spiro-MeOTAD itself, Ag can react with Li-TFSI added as an additive to form Ag-TFSI. The XPS spectrum measured in 0° shows 14.63% of Ag^+ peaks, which indicates that spiro-MeOTAD has more Ag-TFSI. On the other hand, the XPS spectrum of 60° shows 10.56% of Ag^+ peaks, which means that the Ag layer has less Ag-TFSI. It means that a Ag-TFSI layer forms between the bulk spiro-MeOTAD film and the Ag electrode; thus, spiro-MeOTAD becomes de-oxidized. Because of such formation of a multilayer with de-oxidized spiro-MeOTAD and Ag-TFSI at the interface between bulk spiro-MeOTAD and the Ag anode, there is energy level alignment favorable for holes to the anode.[25] In addition, because interfacial Ag turns into Ag^+, the work function of the aged Ag multilayered anode surface increases rather than that of the pristine Ag anode.[26] Here is the proposed chemical equation of spiro-MeOTAD, $TFSI^-$, and Ag in Figure 2f.[24] Another evidence that the oxidation of Ag is due to the reaction with $TFSI^-$ and not due to oxygen can be found in the device aging experiment conducted in the Ar glovebox (Figure S6). Not only the dry air-stored sample but the Ar glovebox-stored sample also showed aging-induced recovery of their performances. This result strongly supported that Ag is oxidized by reacting with $TFSI^-$ without oxygen.

From the measured energy level information of metal electrodes deposited on spiro-MeOTAD in Figure 2, we can propose a detailed reason for the performance recovery in PSCs with Ag electrodes. Energy-level diagram of a PSC can be described as in Figure S7, and we should note that Au has a

DOI: 10.1021/acsami.9b14619
ACS Appl. Mater. Interfaces XXXX, XXX, XXX−XXX

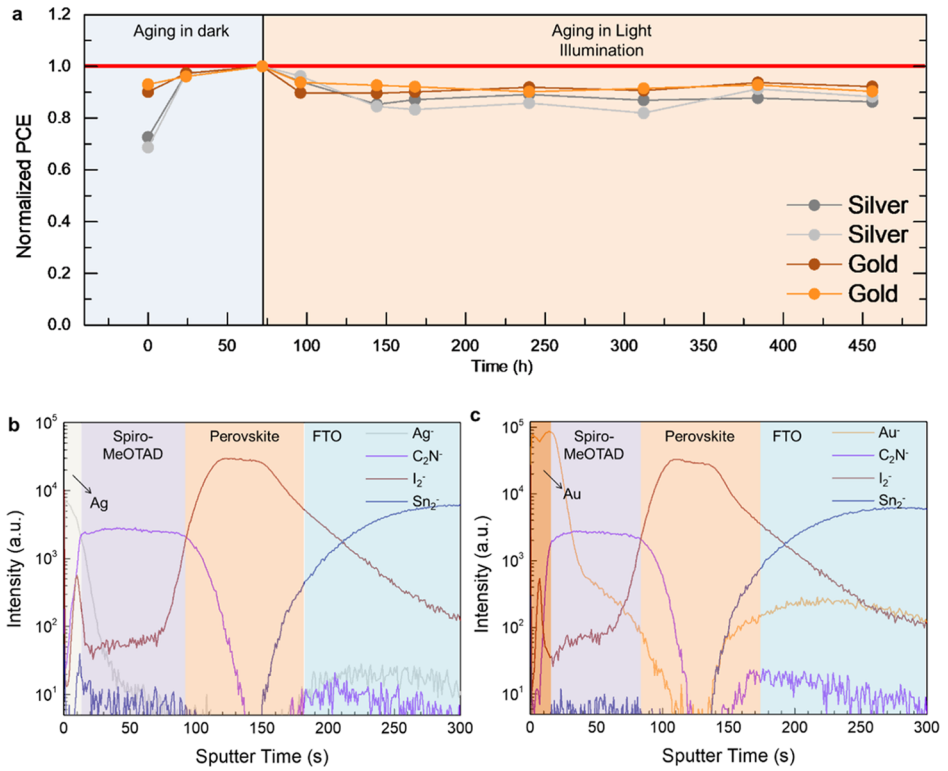

Figure 5. (a) Long-term stability test of Ag and Au metal electrode devices in Ar atmosphere under 1 sun intensity illumination. ToF-SIMS depth profiles of (b) Ag and (c) Au electrode devices after long-term stability tests.

work function of 5.07 eV, which is higher than the spiro-MeOTAD work function (4.9 eV),[25] when the Ag (4.65 eV) has a lower work function than the HTM work function. Therefore, when metal electrodes are deposited on spiro-MeOTAD, there is little upward band bending after the Au electrode deposition, and a hole generated from the perovskite layer is promptly injected into the metal anode pass through the spiro-MeOTAD (Figure 3a). In contrast, as described in Figure 3b, Ag has a value of 4.65 eV, which induces the downward band bending to form a carrier extraction barrier that disturbs hole injection from spiro-MeOTAD to the Ag anode because there is a nonohmic or rectifying contact between the metal and semiconductor when the work function of a p-type semiconductor is larger than that of the metal.[27] The carrier extraction barrier results in an abnormal s-shaped $J-V$ curve, as shown in Figure 1b. However, as we have proved in Figure 2, the Ag anode goes through chemical interaction with Li-TFSI in spiro-MeOTAD after aging, and consequently there is a change in their work function to 5.22 eV, which is now higher than the work function of HTM. Therefore, spiro-MeOTAD has upward band bending after 24 h of aging. The carrier injection barrier is diminished owing to the change in the Ag work function, and the abnormal s-shaped $J-V$ curve is also relieved over time, as shown in Figure 1b.

To verify the energy level transition proposal that the injection barrier influences the performance of the PSCs which plays an important role in the aging-induced performance recovery process, we conducted a $J-V$ curve simulation and compared the similarity between the actual and simulated $J-V$ results. We simulated the $J-V$ curves as functions of the hole injection barrier (Φ_b) from Φ_b = 0.1 to 0.6 eV by changing the anode work function (5.2−4.7 eV), which emulates the PSC system with an Ag electrode. The energy levels for materials are derived from previous literature.[28] All simulations were based on the charge transport equation using the continuity and Poisson's equations.[29] As can be seen in Figure 4a, the poor performance of PSCs with a distinct s-shape gradually recovers to a regular PCE with a high FF as the injection barrier decreases, which shows the same trend as a real device with Ag electrodes, as shown in Figure 1b. In addition to the simulated $J-V$ results, the simulated energy band diagram at $V = V_{OC}$ of low and high hole injection barriers (Φ_b = 0.1 and 0.6 eV) clearly shows a different formation of the junction and energy level alignment between the HTM and metal electrode (Figure 4b,c). The simulated $J-V$ behavior and energy level diagram prove that the poor performance of a device with the Ag electrode at the early stage is mainly attributed to the hole injection barrier, as shown in Figure 3b. Again, the performance recovery with time is evidenced by the work function transition during UPS measurements (Figure 2a,b) and energy level simulation results (Figure 4). Based on simulations, the aging-induced performance recovery in PSCs over time becomes more comprehensive.

Previous discussions show that the formation of the injection barrier because of downward band bending between the oxidized spiro-MeOTAD and Ag electrode results in inferior-performing PSCs. Furthermore, the reduction of oxidized spiro-MeOTAD at the Ag/HTM interface and following the Ag work function shift helped with the aging-induced performance recovery. It indicates that aging for PSCs with Ag electrodes can help with the devices having a comparable performance to PSCs with Au electrodes. In previous research, Ag electrodes have been excluded for use in commercialized electrodes in PSCs owing to a negative perception regarding their performance and chemical stability, such as the easy production of AgI as a by-product.[30] We elucidated the

DOI: 10.1021/acsami.9b14619
ACS Appl. Mater. Interfaces XXXX, XXX, XXX−XXX

fundamentals of the temporary performance instability of the PSCs with Ag electrodes described above. Furthermore, the long-term stability of the recovered devices in an argon atmosphere under 1 sun intensity illumination (white light-emitting diode) to identify their long-term chemical stability was investigated as shown in Figure 5a. Surprisingly, PSCs with Ag electrodes did not show a significant difference in long-term stability to PSCs with Au electrodes. Both devices maintain 85−90% of their initial performance for more than 350 h under continuous light illumination. We also investigated the material transfer or ion migration of both devices using ToF-SIMS after a long-term stability test, as shown in Figure 5b,c. There is no difference in iodide ion migration between the pristine and recovered devices regarding the illumination at both electrodes. According to the results, it can be concluded that Ag, which is much cheaper than Au, is able to be applied in the commercialized PSCs to substitute Au electrodes.

CONCLUSIONS

In this study, different performance alteration trends of PSCs with Ag or Au counter electrodes over time were determined using experimental and simulation methods. First, we observed an s-shaped bend in the current density−voltage curves of PSCs with Ag electrodes immediately after preparation, which achieved their best performance as time progressed, an observation that was not found in devices with Au electrodes. We noticed that such aging-induced recovery phenomena of devices with Ag electrodes, and the different trends depending on the metal electrodes, originate from the injection barrier between the hole transport layer and metal electrodes. Through an in-device electrical characterization (ss-PL), it was clarified that the hole extraction has a significant impact on the s-shaped bend in $J-V$ curves. The work function alignment of HTMs and a metal electrode lead to an inferior hole extraction and s-shaped bend, and we verified why the poor hole extraction and aging-induced recovery process only occurs in devices with Ag electrodes by presenting a variation of the Ag work function as measured using UPS. The chemical mechanism of the Ag work function shift was verified by AR-XPS that present de-oxidized spiro-MeOTAD and Ag-TFSI at the interface between Ag and spiro-MeOTAD. The aging-induced recovery process was completely proved by comparing the experimental $J-V$ results with a $J-V$ curve simulation using the charge continuity equation in accordance with the charge injection barrier. Based on an understanding of the aging process of PSCs with Ag electrodes, we demonstrated a similar long-term stability test under light illumination of both PSCs with Ag and Au electrodes, which was also evidenced by the fact that the ionic composition was not changed during the long-term illumination test. In contrast to previous claims that the Ag electrode is unstable in terms of the device performance as well as chemically, we found that the Ag electrode is one of the most powerful candidates for use in a commercialized electrode in PSCs owing to its low-cost, comparable performance, and chemical stability.

ASSOCIATED CONTENT

Supporting Information

The Supporting Information is available free of charge at https://pubs.acs.org/doi/10.1021/acsami.9b14619.

$J-V$ curves for different aging times, ToF-SIMS depth profiles of pristine and aged devices, $J-V$ curves as HTM precursor oxidation conditions, XPS of HTM as time passes, energy level diagram of PSCs, and $J-V$ characteristics (PDF)

AUTHOR INFORMATION

Corresponding Authors

*E-mail: shmeng@ucsd.edu (Y.S.M.).
*E-mail: hsjung1@skku.edu (H.S.J.).

ORCID

Ying Shirley Meng: 0000-0001-8936-8845
Hyun Suk Jung: 0000-0002-7803-6930

Author Contributions

⊥D.G.L. and M.-c.K. contributed equally to this work.

Notes

The authors declare no competing financial interest.

ACKNOWLEDGMENTS

This work was supported by the Basic Science Research Program through the National Research Foundation of Korea (no. 2017R1A2B3010927), the Global Frontier R&D Program of the Center for Multiscale Energy System (2012M3A6A7054855). This work is also supported by the California Energy Commission EPIC Advance Breakthrough award (EPC-16-050). The XPS and UPS works were performed at the University of California, Irvine Materials Research Institute (IMRI), using instrumentation funded in part by the National Science Foundation Major Research Instrumentation Program under grant CHE-1338173.

REFERENCES

(1) Yang, W. S.; Noh, J. H.; Jeon, N. J.; Kim, Y. C.; Ryu, S.; Seo, J.; Seok, S. I. High-Performance Photovoltaic Perovskite Layers Fabricated through Intramolecular Exchange. *Science* **2015**, *348*, 1234−1237.

(2) Jiang, Q.; Zhang, L.; Wang, H.; Yang, X.; Meng, J.; Liu, H.; Yin, Z.; Wu, J.; Zhang, X.; You, J. Enhanced Electron Extraction Using SnO_2 for High-efficiency Planar-structure $HC(NH_2)_2PbI_3$-based Perovskite Solar Cells. *Nat. Energy* **2016**, *2*, 16177.

(3) Saliba, M.; Matsui, T.; Domanski, K.; Seo, J.-Y.; Ummadisingu, A.; Zakeeruddin, S. M.; Correa-Baena, J.-P.; Tress, W. R.; Abate, A.; Hagfeldt, A.; Gratzel, M. Incorporation of Rubidium Cations into Perovskite Solar Cells Improves Photovoltaic Performance. *Science* **2016**, *354*, 206−209.

(4) Yang, W. S.; Park, B.-W.; Jung, E. H.; Jeon, N. J.; Kim, Y. C.; Lee, D. U.; Shin, S. S.; Seo, J.; Kim, E. K.; Noh, J. H.; Seok, S. I. Iodide Management in Formamidinium-lead-halide−based Perovskite Layers for Efficient Solar Cells. *Science* **2017**, *356*, 1376−1379.

(5) Best Research-Cell Efficiencies. https://www.nrel.gov/pv/assets/pdfs/best-reserch-cell-efficiencies.20190802.pdf (accessed Aug 12, 2019).

(6) Behrouznejad, F.; Shahbazi, S.; Taghavinia, N.; Wu, H.-P.; Wei-Guang Diau, E. A Study on Utilizing Different Metals as the Back Contact of $CH_3NH_3PbI_3$ Perovskite Solar Cells. *J. Mater. Chem. A* **2016**, *4*, 13488−13498.

(7) Chu, Q.-Q.; Ding, B.; Qiu, Q.; Liu, Y.; Li, C.-X.; Li, C.-J.; Yang, G.-J.; Fang, B. Cost Effective Perovskite Solar Cells with a High Efficiency and Open-circuit Voltage Based on a Perovskite-friendly Carbon Electrode. *J. Mater. Chem. A* **2018**, *6*, 8271−8279.

(8) Lee, K.; Kim, J.; Yu, H.; Lee, J. W.; Yoon, C.-M.; Kim, S. K.; Jang, J. A Highly Stable and Efficient Carbon Electrode-based Perovskite Solar Cell Achieved via Interfacial Growth of 2D PEA_2PbI_4 Perovskite. *J. Mater. Chem. A* **2018**, *6*, 24560−24568.

(9) Liu, Y.; Zhao, J.; Li, Z.; Mu, C.; Ma, W.; Hu, H.; Jiang, K.; Lin, H.; Ade, H.; Yan, H. Aggregation and Morphology Control Enables

DOI: 10.1021/acsami.9b14619
ACS Appl. Mater. Interfaces XXXX, XXX, XXX−XXX

Multiple Cases of High-efficiency Polymer Solar Cells. *Nat. Commun.* **2014**, *5*, 5293.
(10) Tress, W.; Petrich, A.; Hummert, M.; Hein, M.; Leo, K.; Riede, M. Imbalanced Mobilities Causing S-shaped IV Curves in Planar Heterojunction Organic Solar Cells. *Appl. Phys. Lett.* **2011**, *98*, 063301.
(11) Oida, T.; Harafuji, K. Attempt to Suppress S-Shaped Kink in Current−Voltage Characteristics in Organic Solar Cells. *Jpn. J. Appl. Phys.* **2013**, *52*, 011601.
(12) Kim, B. J.; Kim, D. H.; Kwon, S. L.; Park, S. Y.; Li, Z.; Zhu, K.; Jung, H. S. Selective Dissolution of Halide Perovskites as a Step Towards Recycling Solar Cells. *Nat. Commun.* **2016**, *7*, 11735.
(13) Domanski, K.; Correa-Baena, J.-P.; Mine, N.; Nazeeruddin, M. K.; Abate, A.; Saliba, M.; Tress, W.; Hagfeldt, A.; Grätzel, M. Not All That Glitters Is Gold: Metal-Migration-Induced Degradation in Perovskite Solar Cells. *ACS Nano* **2016**, *10*, 6306−6314.
(14) Bag, M.; Renna, L. A.; Adhikari, R. Y.; Karak, S.; Liu, F.; Lahti, P. M.; Russell, T. P.; Tuominen, M. T.; Venkataraman, D. Kinetics of Ion Transport in Perovskite Active Layers and Its Implications for Active Layer Stability. *J. Am. Chem. Soc.* **2015**, *137*, 13130−13137.
(15) Wang, S.; Yuan, W.; Meng, Y. S. Spectrum-Dependent Spiro-OMeTAD Oxidization Mechanism in Perovskite Solar Cells. *ACS Appl. Mater. Interfaces* **2015**, *7*, 24791−24798.
(16) Qiu, W.; Buffière, M.; Brammertz, G.; Paetzold, U. W.; Froyen, L.; Heremans, P.; Cheyns, D. High Efficiency Perovskite Solar Cells Using A PCMB/ZnO Double Electron Transport Layer and a Short Air-aging Step. *Org. Electron.* **2015**, *26*, 30−35.
(17) Sundqvist, A.; Sandberg, O. J.; Nyman, M.; Smått, J.-H.; Österbacka, R. Origin of the S-Shaped JV Curve and the Light-Soaking Issue in Inverted Organic Solar Cells. *Adv. Energy Mater.* **2016**, *6*, 1502265.
(18) Kumar, A.; Sista, S.; Yang, Y. Dipole Induced Anomalous S-shape I-V Curves in Polymer Solar Cells. *J. Appl. Phys.* **2009**, *105*, 094512.
(19) Lee, S. T.; Hou, X. Y.; Mason, M. G.; Tang, C. W. Energy Level Alignment at Alq/Metal Interfaces. *Appl. Phys. Lett.* **1998**, *72*, 1593−1595.
(20) Kötz, E. R.; Neff, H.; Müller, K. A UPS, XPS and work function study of emersed silver, platinum and gold electrodes. *J. Electroanul. Chem.* **1986**, *215*, 331−344.
(21) Hornetz, B.; Michel, H.-J.; Halbritter, J. ARXPS Studies of SiO_2-SiC Interfaces and Oxidation of 6H SiC Single Crystal Si-(001) and C-(001) Surfaces. *J. Mater. Res.* **1994**, *9*, 3088−3094.
(22) Pan, J.-M.; Maschhoff, B. L.; Diebold, U.; Madey, T. E. Structural Study of Ultrathin Metal Films on TiO_2, Using LEED, ARXPS and MEED. *Surf. Sci.* **1993**, *291*, 381−394.
(23) Dave, K.; Park, K. H.; Dhayal, M. Two-step Process for Programmable Removal of Oxygen Functionalities of Graphene Oxide: Functional, Structural and Electrical Characteristics. *RSC Adv.* **2015**, *5*, 95657−95665.
(24) Nguyen, W. H.; Bailie, C. D.; Unger, E. L.; McGehee, M. D. Enhancing the Hole-conductivity of Spiro-OMeTAD without Oxygen or Lithium Salts by Using Spiro(TFSI)(2) in Perovskite and Dye-sensitized Solar Cells. *J. Am. Chem. Soc.* **2014**, *136*, 10996−11001.
(25) Harwell, J. R.; Baikie, T. K.; Baikie, I. D.; Payne, J. L.; Ni, C.; Irvine, J. T. S.; Turnbull, G. A.; Samuel, I. D. W. Probing the Energy Levels of Perovskite Solar Cells via Kelvin Probe and UV Ambient Pressure Photoemission Spectroscopy. *Phys. Chem. Chem. Phys.* **2016**, *18*, 19738−19745.
(26) Lang, N. D.; Kohn, W. Theory of Metal Surfaces: Work Function. *Phys. Rev. B: Solid State* **1971**, *3*, 1215−1223.
(27) Barrett, C. R.; Nix, W. D.; Tetelman, A. S. *The Principles of Engineering Materials*; Prentice-Hall, 1973.
(28) Chueh, C.-C.; Li, C.-Z.; Jen, A. K.-Y. Recent Progress and Perspective in Solution-processed Interfacial Materials for Efficient and Stable Polymer and Organometal Perovskite Solar Cells. *Energy Environ. Sci.* **2015**, *8*, 1160−1189.
(29) Calado, P.; Telford, A. M.; Bryant, D.; Li, X.; Nelson, J.; O'Regan, B. C.; Barnes, P. R. Evidence for Ion Migration in Hybrid Perovskite Solar Cells with Minimal Hysteresis. *Nat. Commun.* **2016**, *7*, 13831.
(30) Zhang, T.; Meng, X.; Bai, Y.; Xiao, S.; Hu, C.; Yang, Y.; Chen, H.; Yang, S. Profiling the Organic Cation-dependent Degradation of Organolead Halide Perovskite Solar Cells. *J. Mater. Chem. A* **2017**, *5*, 1103−1111.

DOI: 10.1021/acsami.9b14619
ACS Appl. Mater. Interfaces XXXX, XXX, XXX−XXX